Inclusive h_c production and energy spectrum from e^+e^- annihilation at a super B factory

Qing-Feng Sun,[1,2,*] Yu Jia,[2,†] Xiaohui Liu,[3,‡] and Ruilin Zhu[4,§]

[1]*Department of Modern Physics, University of Science and Technology of China, Hefei, Anhui 230026, China*

[2]*Institute of High Energy Physics, Chinese Academy of Sciences, Beijing 100049, China*

[3]*Center of Advanced Quantum Studies and Department of Physics, Beijing Normal University, Beijing, 100875, China*

[4]*Department of Physics and Institute of Theoretical Physics, Nanjing Normal University, Nanjing, Jiangsu 210023, China*

(Received 25 April 2017; published 30 July 2018)

We calculate the next-to-leading order (NLO) radiative correction to the color-octet h_c inclusive production in e^+e^- annihilation at a super B factory, within the nonrelativistic QCD factorization framework. The analytic expression for the NLO short-distance coefficient (SDC) accompanying the color-octet production operator $\mathcal{O}_8^{h_c}(^1S_0)$ is obtained after summing both virtual and real corrections. The size of NLO correction for the color-octet production channel is found to be positive and substantial. The NLO prediction to the h_c energy spectrum is plagued with unphysical end-point singularity. With the aid of the soft-collinear effective theory, those large end-point logarithms are resummed to the next-to-leading logarithmic (NLL) accuracy. Consequently, further supplemented with the nonperturbative shape function, we obtain the well-behaved predictions for the h_c energy spectrum in the entire kinematic range, which awaits examination by the forthcoming Belle II experiment.

DOI: 10.1103/PhysRevD.98.014039

I. INTRODUCTION

The $h_c(1P)$ meson, the lowest-lying spin-singlet P-wave charmonium, is the last member found among the charmonium family below the open charm threshold. The first hint about its existence was reported in the process $p\bar{p} \to h_c \to J/\psi\pi^0$ by the Fermilab E760 experiment in 1992 [1]. Finally, in 2005, the h_c state was firmly established through the process $p\bar{p} \to h_c \to \eta_c\gamma$ in the Fermilab E835 experiment [2], as well as through the isospin-violating charmonium transition process $\psi(2S) \to h_c(\to \eta_c\gamma) + \pi^0$ in the CLEO-c experiment [3,4]. Later, this decay chain was confirmed in the BESIII experiment with a much greater data sample [5,6]. To date, the latest measured mass and width of h_c are $M_{h_c} = 3525.38 \pm 0.11$ MeV and $\Gamma_{h_c} = 0.7 \pm 0.28 \pm 0.22$ MeV, respectively [7]. Two exclusive decay channels, the electric dipole ($E1$) radiative transition $h_c \to \eta_c\gamma$ and the Okubo-Zweig-Iizuka (OZI)-suppressed annihilation decay $h_c \to 2\pi^+2\pi^-\pi^0$, have been measured, with the corresponding branching fractions $\mathcal{B}(h_c \to \eta_c\gamma) = (51 \pm 6)\%$ and $\mathcal{B}(h_c \to 2\pi^+2\pi^-\pi^0) = (2.2^{+0.8}_{-0.7})\%$, respectively [7]. It is worth mentioning that the $^1P_1$ counterparts in the bottomonium family, the $h_b(1P, 2P)$ mesons, have also recently been established via the di-pion transition from the $\Upsilon(5S)$ resonance in the Belle experiment [8].

It is interesting to ask whether one can possibly understand various dynamical aspects of the h_c meson from the first principles of QCD. In fact, nonrelativistic QCD (NRQCD) [9], the modern effective field theory to describe the slowly moving heavy quark–antiquark system, is an appropriate model-independent framework to tackle a multiscale system exemplified by the charmonium state h_c. Furthermore, the NRQCD factorization approach [10], originally developed by Bodwin *et al.*, provides a powerful and systematic language to describe the inclusive quarkonium production and decay processes that has been fruitfully applied to uncountable charmonium phenomenologies in the past two decades [11].

For the dominant $E1$ decay process $h_c \to \eta_c\gamma$, there have been many preceding studies based on the multipole expansion picture in the quark potential models [12]. Moreover, the radiative and relativistic corrections to the inclusive hadronic widths of $h_{c,b}$ have recently been investigated in the NRQCD factorization framework [13]. On the other hand, h_c production in various collision environments has also been extensively investigated in recent years. For instance, h_c inclusive production in B

*qfsun@mail.ustc.edu.cn
†jiay@ihep.ac.cn
‡xiliu@bnu.edu.cn
§rlzhu@njnu.edu.cn

meson decay [14,15]; h_c photoproduction [16]; h_c hadroproduction [17–19]; inclusive h_c production from e^+e^- annihilation [20,21]; and exclusive h_c production from Z^0 decay [22], from double charmonium production in e^+e^- annihilation [23], and from $\Upsilon(nS)$ decay [24].

The hadroproduction rate of h_c is significant at the LHC experiment due to the huge partonic luminosity. A recent computation indicates that the gluon-to-h_c fragmentation probability may reach the order 10^{-6} [25]. In sharp contrast to $J/\psi(\psi')$ hadroproduction [26–30], unfortunately it is rather challenging to reconstruct the h_c events via the dominant decay channel $h_c \to \eta_c\gamma$, due to the tremendous background at hadron collision experiments. In contrast, tagging h_c is much more tractable in the e^+e^- machines than in hadron colliders. For example, the exclusive h_c production process $e^+e^- \to h_c\pi^+\pi^-$ at center-of-mass energy $\sqrt{s} = 4.170$ GeV has been studied by the CLEO Collaboration, with the cross section measured to be $15.6 \pm 2.3 \pm 1.9 \pm 3.0$ pb [31]. They also found evidence for the process $e^+ + e^- \to h_c\eta$ at the 3σ confidence level. As a byproduct of studying this exclusive h_c production channel, BESIII have recently found two charmoniumlike resonances, namely, the $Y(4220)$ and $Y(4390)$ [32].

The forthcoming Belle II experiment (also referred to as a super B factory) will accumulate a tremendous data set near the $\Upsilon(4S)$ energy. In this paper, we will focus on the inclusive h_c production in e^+e^- annihilation at $\sqrt{s} \approx 10.58$ GeV, near the $\Upsilon(4S)$ resonance. In the previous work [20,21], the NRQCD SDCs were evaluated for both color-singlet and color-octet channels at the leading order (LO) in α_s, and it was found that the latter octet-channel production cross section dominated the singlet-channel cross section. Therefore, in order to make a more precise prediction, it is helpful to evaluate the next-to-leading order (NLO) QCD correction to the color-octet cross section. Moreover, to expedite the experimental search for h_c, it is crucial to predict not only the total h_c production rate, but also the differential h_c energy spectrum.

The LO color-octet contribution to the h_c energy spectrum in $e^+e^- \to h_c + X$ is simply a δ-function, determined by the partonic process $e^+e^- \to c\bar{c}({}^1S_0^{(8)}) + g$. After including the real correction in the color-octet channel, $e^+e^- \to c\bar{c}({}^1S_0^{(8)}) + gg$, the energy spectrum then becomes continuous over the entire allowed domain; however, it turns out to be singular near the upper end point, due to the soft and collinear gluon radiation in this limited region of phase space. This signals a breakdown of the fixed-order QCD prediction, and failure of NRQCD expansion near this kinematic end-point region. The aim of this work is thus twofold. First we extend the LO color-octet NRQCD SDC obtained in [20] to NLO in α_s, in a fully analytical manner. Secondly, we follow the recipe of the resumming large logarithms in the color-octet channel for the process $e^+e^- \to J/\psi + X$ near the end-point region [33], which was formulated in the context of the soft-collinear effective theory (SCET) [34–39], to tame the end-point singularity encountered in our case, and finally predict a well-behaved h_c energy spectrum. We hope our prediction will provide some useful guidance for unambiguously erecting the h_c state in the forthcoming Belle II experiment.

The rest of the paper is distributed as follows. In Sec. II, the fixed-order calculations for the short-distance coefficients (SDCs) are presented within the NRQCD factorization framework. We first review the existing LO results for both color-singlet and octet channels. In Sec. III, we present the analytical expressions for NLO NRQCD SDCs from the color-octet channel, including both virtual and real corrections. In Sec. IV, within the SCET framework, we show how to resum the large endpoint logarithms to the next-to-leading logarithmic (NLL) accuracy. In Sec. V, we present our numerical results for the total h_c production rate and its differential energy spectrum. We also discuss the observational prospects of the $h_c(1P, 2P)$ states in the forthcoming Belle II experiment. Finally we summarize in Sec. VI. In the Appendix, we expound how to analytically carry out the three-body phase space to isolate the soft and collinear divergences in $d = 4 - 2\epsilon$ spacetime dimensions.

II. NRQCD FACTORIZATION AND LO SHORT-DISTANCE COEFFICIENTS

A. NRQCD factorization for h_c production

Heavy quarkonium is a QCD bound state predominantly composed of a pair of a nonrelativistic heavy quark and antiquark. For the charmonium, the typical velocity between the charm quarks inside a charmonium is roughly $v^2 \approx 0.3$; thus, velocity expansion is not anticipated to converge very well. According to the NRQCD factorization theorem [10], the inclusive production rate of h_c can be expressed as a sum of the product of perturbatively calculable NRQCD SDCs and the nonperturbative NRQCD long-distance matrix elements (LDMEs). The importance of the LDMEs is weighed by the power counting in v. At the lowest order in v, the differential cross section for inclusive h_c production can be written as [10]

$$d\sigma[e^+e^- \to h_c + X] = \frac{dF_1(\mu_\Lambda)}{m_c^4}\langle \mathcal{O}_1^{h_c}({}^1P_1)\rangle + \frac{dF_8}{m_c^2}\langle \mathcal{O}_8^{h_c}({}^1S_0)(\mu_\Lambda)\rangle + \cdots, \quad (1)$$

where the SDCs dF_1 and dF_8 can be calculated order by order in α_s, and $\langle \mathcal{O}_1^{h_c}({}^1P_1)\rangle$ and $\langle \mathcal{O}_8^{h_c}({}^1S_0)\rangle$ are the color-singlet and color-octet NRQCD production LDMEs,

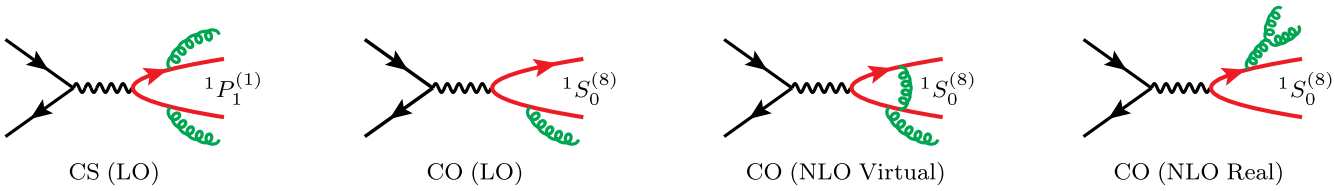

FIG. 1. Representative Feynman diagrams for the $c\bar{c}(n)$ production from e^+e^- annihilation, for $n = {}^1S_0^{(8)}$ or ${}^1P_1^{(1)}$.

respectively. The corresponding h_c production operators in NRQCD are defined as [10][1]

$$\mathcal{O}_1^{h_c}({}^1P_1) = \chi^\dagger\left(-\frac{i}{2}\overleftrightarrow{\mathbf{D}}\right)\psi\sum_X|h_c+X\rangle \cdot\langle h_c+X|\psi^\dagger\left(-\frac{i}{2}\overleftrightarrow{\mathbf{D}}\right)\chi, \tag{2a}$$

$$\mathcal{O}_8^{h_c}({}^1S_0) = \chi^\dagger T^a\psi\sum_X|h_c+X\rangle\cdot\langle h_c+X|\psi^\dagger T^a\chi, \tag{2b}$$

where ψ and χ denote the Pauli spinor fields that annihilate a heavy quark and create a heavy antiquark, respectively. $\overleftrightarrow{\mathbf{D}}$ represents the left-right symmetric spatial component of the covariant derivative $D_\mu = \partial_\mu - ig_sT^aA_\mu^a$, and T^a $(a = 1,\ldots,8)$ signifies the generator in the fundamental representation of the $SU(3)_c$ group. The μ_Λ refers to the NRQCD factorization scale, which lies in the range $m_cv \le \mu_\Lambda \le m_c$. These two NRQCD production operators are interconnected through the NRQCD renormalization group equation (RGE) [10]:

$$\frac{d}{d\ln\mu_\Lambda^2}\langle\mathcal{O}_8^{h_c}({}^1S_0)(\mu_\Lambda)\rangle = \frac{2C_F\alpha_s(\mu_\Lambda)}{3\pi N_cm_c^2}\langle\mathcal{O}_1^{h_c}({}^1P_1)\rangle. \tag{3}$$

Being infrared finite, dF_1 and dF_8 are insensitive to the long-distance hadronization effects and thus can be determined through the standard perturbative matching procedure. One can replace the physical h_c state in Eq. (1) by the free on-shell $c\bar{c}$ pairs with quantum numbers ${}^1S_0^{(8)}$ or ${}^1P_1^{(1)}$, computing both sides of Eq. (1), demanding both perturbative QCD and perturbative NRQCD to generate identical results. Ultimately, one can solve these two linear equations to ascertain the two SDCs, order by order in α_s. Here we stress that it is crucial to include the color-octet contribution; otherwise the uncanceled IR divergences emerging from the color-singlet channel would impede the predictive power of NRQCD. For the computation in the QCD side, it is convenient to employ the covariant projection technique [42,43] to project the $c\bar{c}$ amplitude onto the intended ${}^{2S+1}L_J$ states. Throughout this work, dimensional regularization (DR), that is, to work in the spacetime dimensions $d = 4-2\epsilon$, is adopted to regularize both UV and IR divergences.

A kinematical simplification also arises from the s-channel nature of this process. As long as we are concerned only with the h_c energy distribution, one can reexpress the h_c production rate from e^+e^- annihilation in terms of that from virtual photon decay [44]:

$$d\sigma[e^+e^-\to h_c+X] = \frac{4\pi\alpha}{s^{3/2}}d\Gamma[\gamma^*\to h_c+X], \tag{4}$$

where the center-of-mass energy of the e^+e^- system is denoted by $\sqrt{s}$.

Some representative Feynman diagrams for $c\bar{c}(n)$ $[n = {}^1S_0^{(8)}$ or ${}^1P_1^{(1)}]$ production from e^+e^- annihilation in both color-singlet and color-octet channels are shown in Fig. 1. Due to the odd C parity of the h_c meson, the color-singlet channel starts at $\mathcal{O}(\alpha_s^2)$, while the octet contribution starts at $\mathcal{O}(\alpha_s)$. In the rest of this section, we will briefly review the LO results for F_8 and F_1, which were first analytically evaluated in Ref. [20].

B. LO color-octet SDC

At LO in the color-octet channel, we only need to consider $e^+e^-\to\gamma^*\to c\bar{c}({}^1S_0^{(8)})+g$. The differential two-body phase space in $d = 4-2\epsilon$ dimensions reads [20]

$$d\Phi_2 = \frac{c_\epsilon}{8\pi}s^{-\epsilon}(1-r)^{1-2\epsilon}\delta(1+r-z)dz, \tag{5}$$

where

$$c_\epsilon \equiv (4\pi)^\epsilon\frac{\Gamma(1-\epsilon)}{\Gamma(2-2\epsilon)}, \qquad r\equiv\frac{4m_c^2}{s}, \qquad z\equiv\frac{2P^0}{\sqrt{s}}, \tag{6}$$

with $P^\mu = (P^0,\mathbf{P})$ representing the four-momentum of the $c\bar{c}$ pair.

The LO amplitude squared turns out to be

$$\sum_{\text{Pol,Col}}|\mathcal{M}^{(0)}[\gamma^*\to c\bar{c}({}^1S_0^{(8)})+g]|^2 = 256\pi^2e_c^2\alpha C_AC_F\alpha_s\mu_r^{2\epsilon}(1-\epsilon)(1-2\epsilon), \tag{7}$$

[1]It was first made clear by Nayak *et al.* [40,41] a decade ago that the original definition of the NRQCD color-octet production operator [10] is not gauge invariant, and the correct definition necessitates the inclusion of eikonal lines that run from the location of the quark/antiquark fields to infinity. To the perturbative order considered in this work, this nuisance does not play a role so we adhere to the conventional definition [10].

where $e_c = \frac{2}{3}$ is the electric charge of the charm quark, and $C_A = 3$ and $C_F = \frac{4}{3}$ are the Casimirs of the color $SU(3)_c$ group. Integrating Eq. (7) over the two-body phase space in Eq. (5), we obtain

$$\hat{\sigma}_{\rm LO}^{(8)} \equiv \frac{2\pi\alpha}{3s^2}\int d\Phi_2 \sum_{\rm Pol,Col} |\mathcal{M}^{(0)}[\gamma^* \to c\bar{c}(^1S_0^{(8)}) + g]|^2 = \left(\frac{4\pi\mu_r^2}{s}\right)^{\epsilon} \frac{\Gamma(2-\epsilon)}{\Gamma(1-2\epsilon)} \frac{64\pi^2 e_c^2 \alpha^2 C_A C_F \alpha_s (1-r)^{1-2\epsilon}}{3s^2}. \tag{8}$$

The factor $\frac{1}{3}$ accounts for averaging over the three polarizations of γ^*. The differential expression of $\hat{\sigma}_{\rm LO}^{(8)}$ in four dimensions reads

$$\left.\frac{d\hat{\sigma}_{\rm LO}^{(8)}}{dz}\right|_{d\to 4} = \frac{64\pi^2 e_c^2 \alpha^2 C_A C_F \alpha_s (1-r)}{3s^2}\delta(1+r-z). \tag{9}$$

Substituting Eq. (9) into the left-hand side of Eq. (1), and only retaining the NRQCD matrix element in the color-octet channel, we then deduce the LO color-octet SDC:

$$\frac{dF_8^{\rm LO}}{dz} = \frac{m_c}{\langle \mathcal{O}_8^{c\bar{c}}(^1S_0)\rangle}\frac{d\hat{\sigma}_{\rm LO}^{(8)}}{dz} = \frac{64\pi^2 e_c^2 \alpha^2 C_A C_F \alpha_s (1-r) m_c}{3(N_c^2-1)s^2}\delta(1+r-z), \tag{10}$$

where we have used $\langle \mathcal{O}_8^{c\bar{c}}(^1S_0)\rangle = N_c^2 - 1$. The integrated color-octet SDC is then

$$F_8^{\rm LO} = \frac{64\pi^2 e_c^2 \alpha^2 C_A C_F \alpha_s (1-r) m_c}{3(N_c^2-1)s^2}, \tag{11}$$

which scales as $1/s^2$ asymptotically.

C. LO color-singlet SDC

To determine the LO SDC in the color-singlet channel, we need to consider the partonic process $e^+e^- \to c\bar{c}(^1P_1^{(1)}) + gg$. The IR divergence appears in the upper end point of the h_c spectrum, when one of the gluons becomes soft. It is most convenient to handle this IR singularity using DR. As a virtue of the color-octet mechanism of NRQCD, the single IR pole is factored into the color-octet NRQCD LDME. As a remnant of this IR divergence, the renormalized color-octet LDME is defined at the NRQCD factorization scale μ_Λ; in the meantime, the SDC F_1 acquires an explicit logarithmic dependence on μ_Λ. The differential color-singlet SDC dF_1/dz is somewhat too lengthy to reproduce here, and we refer interested readers to Ref. [20] for its complete expression. Here we just present the integrated color-singlet SDC:

$$F_1^{\rm LO}(\mu_\Lambda) = \frac{64\pi e_c^2 \alpha^2 C_F \alpha_s^2 m_c}{9N_c s^2}(1-r)\left[-\ln\frac{\mu_\Lambda^2}{4m_c^2} + 2\ln(1-r) - \frac{65-84r}{12(1-r)} + \frac{7+7r-9r^2}{6(1-r)^2}\ln r + \frac{r(5-7r)}{16(1-r)^2}\ln^2\frac{1+\sqrt{1-r}}{1-\sqrt{1-r}} + \frac{14-15r}{8(1-r)^{3/2}}\ln\frac{1+\sqrt{1-r}}{1-\sqrt{1-r}}\right], \tag{12}$$

which is obtained according to the $\overline{\rm MS}$ renormalization scheme. It is enlightening to see the asymptotic behavior of $F_1^{\rm LO}$ in the $\sqrt{s} \gg m_c$ limit:

$$F_1^{\rm LO}(\mu_\Lambda)|_{\rm Asym} = \frac{64\pi e_c^2 \alpha^2 C_F \alpha_s^2 m_c}{9N_c s^2}\left(-\frac{7}{12}\ln r - \ln\frac{\mu_\Lambda^2}{4m_c^2} - \frac{65}{12} + \frac{7}{2}\ln 2\right), \tag{13}$$

which is proportional to $1/s^2$ times a single logarithm of s/m_c^2.

III. NLO RADIATIVE CORRECTION FOR THE COLOR-OCTET CHANNEL

In this section, we are going to calculate the NLO radiative correction for the color-octet SDC dF_8, which includes the real correction $e^+e^- \to c\bar{c}(^1S_0^{(8)}) + gg(q\bar{q})$, together with the one-loop virtual correction to $e^+e^- \to c\bar{c}(^1S_0^{(8)}) + g$. The UV divergences encountered in virtual correction will be eliminated by the standard renormalization procedure, while the IR singularities turn out to cancel out after summing both real and virtual corrections.

In the NLO calculation, we generate the QCD Feynman diagrams and amplitudes using the package FeynArts [45], and employ the package FeynCalc [46] to carry out contraction of the Lorentz indices and trace over Dirac matrices. We use the Feynman gauge throughout the calculation.

A. Real correction

There are more Feynman diagrams for $e^+e^- \to \gamma^* \to c\bar{c}(^1S_0^{(8)}) + gg$ than the color-singlet channel, since the

three-gluon vertex is permitted due to the color-octet feature of the $c\bar{c}$ pair. Furthermore, the new channel $e^+e^- \to \gamma^* \to c\bar{c}({}^1S_0^{(8)}) + q\bar{q}$ also becomes permissible. One typical real emission diagram is depicted in Fig. 1.

In this section, we will quickly present the analytic results by integrating the squared amplitudes over the three-body phase space in DR, closely following the recipe outlined in Ref. [20]. To ensure the correctness of our results, we also redo the calculation using a numerical recipe, i.e., utilizing the two-cutoff phase space slicing method [47], and find full agreement with our analytical results.

First, let us introduce, in addition to z, two additional fractional energy variables, x_1 and x_2:

$$x_1 \equiv \frac{2k_1^0}{\sqrt{s}}, \qquad x_2 \equiv \frac{2k_2^0}{\sqrt{s}}, \tag{14}$$

where k_1 and k_2 represent the momenta of the final-state gluons (or light quark and antiquark) in a real emission process. These variables are subject to the constraint $x_1 + x_2 + z = 2$ by energy conservation.

For convenience, we separate the squared amplitude for $\gamma^* \to c\bar{c}({}^1S_0^{(8)}) + gg$ into four pieces:

$$\sum_{\text{Pol,Col}} \left|\mathcal{M}^{\text{R}}[\gamma^* \to c\bar{c}({}^1S_0^{(8)}) + gg]\right|^2 = \mathcal{I}_{\text{S}}(x_i, z) + \mathcal{I}_{\text{C}}(x_i, z) + \mathcal{I}_{\text{SC}}(x_i, z) + \mathcal{I}_{\text{Fin}}(x_i, z), \tag{15}$$

with $i = 1, 2$. Explicitly, these four pieces are

$$\mathcal{I}_{\text{S}}(x_i, z) = -\frac{2^{12}\pi^3 e_c^2 \alpha C_A^2 C_F \alpha_s^2 \mu_r^{4\epsilon}(1-\epsilon)(1-2\epsilon) r}{s}\left[\frac{1}{(1+r-z-x_1)^2} + \frac{1}{(1+r-z-x_2)^2}\right], \tag{16a}$$

$$\mathcal{I}_{\text{C}}(x_i, z) = \frac{2^{12}\pi^3 e_c^2 \alpha C_A^2 C_F \alpha_s^2 \mu_r^{4\epsilon}(1-\epsilon)(1-2\epsilon)}{(1-r)^2 s}\frac{x_1 x_2 - 2(1-r)^2}{1+r-z}, \tag{16b}$$

$$\mathcal{I}_{\text{SC}}(x_i, z) = -\frac{2^{12}\pi^3 e_c^2 \alpha C_A^2 C_F \alpha_s^2 \mu_r^{4\epsilon}(1-\epsilon)(1-2\epsilon)(1-r)}{s}\frac{1}{1+r-z}\left(\frac{1}{1+r-z-x_1} + \frac{1}{1+r-z-x_2}\right), \tag{16c}$$

$$\begin{aligned}\mathcal{I}_{\text{Fin}}(x_i, z) = {} & \frac{2^{12}\pi^3 e_c^2 \alpha C_A^2 C_F \alpha_s^2}{(1-r)^2(2-z)^2(1-r-x_1)^2(1-r-x_2)^2 s}\{(1-r)^3(1+r-z)(z-2r)(2-z)^2 \\ & - (1-r)^3(5+2r+r^2-5z-rz+z^2)x_1 x_2 + 2(1-r)(2-z)^2 x_1^2 x_2^2 - (3-r-z)x_1^3 x_2^3\}.\end{aligned} \tag{16d}$$

Each individual term is symmetric under the exchange $x_1 \leftrightarrow x_2$, reflecting the Bose symmetry of the two gluons in the final state. Upon phase space integration, the first term $\mathcal{I}_{\text{S}}$ would lead to a single soft pole, when one of the gluons becomes soft. The second term $\mathcal{I}_{\text{C}}$ would result in a single collinear pole, when the final-state gluons become collinear to each other. The third term $\mathcal{I}_{\text{SC}}$ would produce the double IR pole, arising from the corner of phase space where one of the gluons becomes simultaneously soft and collinear to the other one. Note both soft and collinear singularities can arise only when the $c\bar{c}$ pair acquires its maximal energy, that is, in the $z \to 1 + r$ limit. The last term $\mathcal{I}_{\text{Fin}}$ will not result in any IR divergences upon phase space integration and therefore can be directly treated in four spacetime dimensions.

Integrating the squared amplitudes in Eq. (15) over the three-body phase space, we obtain

$$\hat{\sigma}_{\text{R}}^{(8),gg} \equiv \hat{\sigma}_{\text{Div}}^{(8),gg} + \hat{\sigma}_{\text{Fin}}^{(8),gg}, \tag{17}$$

where the "divergent" and "finite" partonic cross sections are defined as

$$\begin{aligned}\hat{\sigma}_{\text{Div}}^{(8),gg} &= \int_{2\sqrt{r}}^{1+r} dz \frac{d\hat{\sigma}_{\text{Div}}^{(8),gg}}{dz} \\ &= \frac{1}{2!}\frac{2\pi\alpha}{3s^2}\int d\Phi_3[\mathcal{I}_{\text{S}}(x_i, z) + \mathcal{I}_{\text{C}}(x_i, z) + \mathcal{I}_{\text{SC}}(x_i, z)],\end{aligned} \tag{18a}$$

$$\hat{\sigma}_{\text{Fin}}^{(8),gg} = \int_{2\sqrt{r}}^{1+r} dz \frac{d\hat{\sigma}_{\text{Fin}}^{(8),gg}}{dz} = \frac{1}{2!}\frac{2\pi\alpha}{3s^2}\int d\Phi_3 \mathcal{I}_{\text{Fin}}(x_i, z). \tag{18b}$$

Here $d\Phi_3$ signifies the three-body phase space measure, whose exact definition in $d = 4 - 2\epsilon$ dimensions is given in Eq. (A1). We have also included a symmetry factor $\frac{1}{2!}$ in Eq. (18), to account for the indistinguishability of the final-state gluons.

By carrying out one-fold integration over x_1 in Eq. (18), we then arrive at the partonic cross section differential in the energy fraction of the $c\bar{c}$ pair:

$$\frac{d\hat{\sigma}^{(8),gg}_{\rm Div}}{dz} = \hat{\sigma}^{(8)}_{\rm LO}\frac{\alpha_s}{\pi}\frac{(1-r)^{-2\epsilon}r^{\epsilon}}{\Gamma(1-\epsilon)}\left(\frac{4\pi\mu_r^2}{s}\right)^{\epsilon}\times C_A\Bigg\{\left(\frac{1}{2\epsilon^2}+\frac{17}{12}\frac{1}{\epsilon}-2\ln^2\frac{\sqrt{r}}{1+\sqrt{r}}-\frac{23}{6}\ln\frac{\sqrt{r}}{1+\sqrt{r}}-\frac{\pi^2}{4}+\frac{67}{36}\right)\delta(1+r-z)$$
$$+\left[\frac{1}{1+r-z}\right]_+\left[2\ln\frac{2-z+\sqrt{z^2-4r}}{2}-\ln\frac{z-\sqrt{z^2-4r}}{z+\sqrt{z^2-4r}}-\frac{2\sqrt{z^2-4r}}{1-r}+\frac{\sqrt{z^2-4r}(6+2r-6z+z^2)}{12(1-r)^3}\right]$$
$$-\left[\frac{\ln(1+r-z)}{1+r-z}\right]_+\Bigg\}, \tag{19a}$$

$$\frac{d\hat{\sigma}^{(8),gg}_{\rm Fin}}{dz} = \hat{\sigma}^{(8)}_{\rm LO}\frac{\alpha_s}{\pi}\frac{C_A}{12(1-r)^3(z-2r)^3(2-z)^2}\Bigg\{\sqrt{z^2-4r}[16r(3-9r+9r^2+24r^3-28r^4+9r^5)$$
$$-8(3-3r-9r^2+120r^3-94r^4+27r^5)z+4(6-15r+162r^2-75r^3+22r^4)z^2$$
$$-2(3+90r+23r^2+4r^3)z^3+2(12+25r+3r^2)z^4-(9+5r)z^5+z^6]$$
$$+12(1-r)^2\ln\frac{z-2r-\sqrt{z^2-4r}}{z-2r+\sqrt{z^2-4r}}[4r(1-2r-6r^2+2r^3-3r^4)+8r^2(6+r+3r^2)z$$
$$-2(1+12r+15r^2+12r^3)z^2+2(3+9r+8r^2)z^3-2(2+3r)z^4+z^5]\Bigg\}, \tag{19b}$$

where $\hat{\sigma}^{(8)}_{\rm LO}$ is given in Eq. (8).

From Eq. (19a), one immediately sees that the double and single IR poles indeed occur exactly at the location $z = 1 + r$. The "+"-function in Eq. (19a) is understood in the distributive sense, i.e.,

$$\int_{2\sqrt{r}}^{1+r} dz[f(z)]_+ g(z) = \int_{2\sqrt{r}}^{1+r} dz f(z)[g(z) - g(1+r)], \tag{20}$$

where $g(z)$ is an arbitrary test function that is regular at $z = 1 + r$.

Obtaining the analytic expressions in Eq. (19) requires more effort than in the color-singlet channel, since a double IR pole emerges in our case, whereas only a single soft pole occurs in that case [20]. Some technical details about isolating IR singularities with the DR method are expounded in Appendix.

Further integrating Eq. (19) over the entire range of z, we then obtain the integrated partonic cross section for $e^+e^- \to c\bar{c}({}^1S_0^{(8)}) + gg$:

$$\hat{\sigma}^{(8),gg}_{\rm R} = \hat{\sigma}^{(8)}_{\rm LO}\frac{\alpha_s}{\pi}\frac{(1-r)^{-2\epsilon}r^{\epsilon}}{\Gamma(1-\epsilon)}\left(\frac{4\pi\mu_r^2}{s}\right)^{\epsilon}C_A\left[\frac{1}{2\epsilon^2}+\frac{17}{12}\frac{1}{\epsilon}+\frac{2-3r}{16(1-r)}\ln^2\frac{1-\sqrt{1-r}}{1+\sqrt{1-r}}\right.$$
$$\left.+\,{\rm Li}_2\left(-\frac{1-r}{r}\right)+\frac{10-9r}{12(1-r)^{3/2}}\ln\frac{1-\sqrt{1-r}}{1+\sqrt{1-r}}+\frac{1-6\ln r}{6(1-r)}+\frac{235}{36}-\frac{5\pi^2}{12}\right]. \tag{21}$$

We can carry out the real correction calculation for $\gamma^* \to c\bar{c}({}^1S_0^{(8)}) + q\bar{q}$ in a similar vein. The squared amplitude in d dimensions reads

$$\sum_{u,d,s}\sum_{\rm Pol,Col}|\mathcal{M}^{\rm R}[\gamma^* \to c\bar{c}({}^1S_0^{(8)}) + q\bar{q}]|^2 = \frac{2^{10}\pi^3 e_c^2\alpha C_A C_F n_f \alpha_s^2\mu_r^{4\epsilon}(1-2\epsilon)}{(2-z)^2(1+r-z)s}\times[x_1^2+x_2^2-2(1+r-z)-\epsilon(z^2-4r)], \tag{22}$$

where $n_f = 3$ represents the number of light flavors, where only u, d, and s are retained. The light quarks are treated as massless. After integrating Eq. (22) over the energy fraction of the massless quark, x_1, we obtain

$$\frac{d\hat{\sigma}_{\rm R}^{(8),q\bar{q}}}{dz}=\hat{\sigma}_{\rm LO}^{(8)}\frac{\alpha_s}{\pi}\frac{(1-r)^{-2\epsilon}r^{\epsilon}}{\Gamma(1-\epsilon)}\left(\frac{4\pi\mu_r^2}{s}\right)^{\epsilon}\times\frac{n_f}{6}\left\{\left[-\frac{1}{\epsilon}+2\ln\frac{\sqrt{r}}{1+\sqrt{r}}-\frac{5}{3}\right]\delta(1+r-z)+\left[\frac{1}{1+r-z}\right]_+\frac{(z^2-4r)^{3/2}}{(1-r)(2-z)^2}\right\}. \tag{23}$$

Unlike the case for $e^+e^-\to c\bar{c}({}^1S_0^{(8)})+gg$, here only the single pole arises, originating from the configuration where the light quark and antiquark become collinear.

The integrated expression for $\hat{\sigma}_{\rm R}^{(8),q\bar{q}}$ turns out to be

$$\hat{\sigma}_{\rm R}^{(8),q\bar{q}}=\hat{\sigma}_{\rm LO}^{(8)}\frac{\alpha_s}{\pi}\frac{(1-r)^{-2\epsilon}r^{\epsilon}}{\Gamma(1-\epsilon)}\left(\frac{4\pi\mu_r^2}{s}\right)^{\epsilon}\times\frac{n_f}{6}\left(-\frac{1}{\epsilon}-\frac{20-8r-9\ln r}{3(1-r)}-\frac{2}{(1-r)^{3/2}}\ln\frac{1-\sqrt{1-r}}{1+\sqrt{1-r}}\right). \tag{24}$$

B. Virtual correction

In order to render finite predictions, one should further consider the virtual correction to $e^+e^-\to c\bar{c}({}^1S_0^{(8)})+g$, which also contains IR singularities that serve to cancel those IR singularities encountered in the real correction, as encoded in Eqs. (19) and (23).

One typical one-loop diagram is depicted in Fig. 1. The partial fraction in the one-loop amplitudes is conducted with the aid of the package \$Apart [48], and the integration-by-part reduction is facilitated by the package FIRE [49]. The resulting master integrals (MIs) are then calculated analytically, whose correctness is also numerically verified by the package LoopTools [50]. After the renormalization of the charm quark mass as well as the QCD coupling constant, the UV divergences in the one-loop QCD amplitude will be eliminated.

Squaring the amplitudes and integrating over the two-body phase space, we obtain

$$\hat{\sigma}_{\rm V}^{(8)}\equiv\int_{2\sqrt{r}}^{1+r}dz\frac{d\hat{\sigma}_{\rm V}^{(8)}}{dz}=\frac{2\pi\alpha}{3s^2}\int d\Phi_2\sum_{\rm Pol,Col}2{\rm Re}\{\mathcal{M}^{(0)}[\gamma^*\to c\bar{c}({}^1S_0^{(8)})+g]\mathcal{M}^{(1)}[\gamma^*\to c\bar{c}({}^1S_0^{(8)})+g]\}, \tag{25}$$

where $\mathcal{M}^{(0)}$ denotes the tree-level amplitude for $\gamma^*\to c\bar{c}({}^1S_0^{(8)})+g$, and $\mathcal{M}^{(1)}$ represents the order-α_s one-loop QCD amplitude. After substituting the analytical expressions for the MIs, and including the counterterm diagrams, we are able to deduce the differential expression analytically for the virtual correction:

$$\begin{aligned}\frac{d\hat{\sigma}_{\rm V}^{(8)}}{dz}=\hat{\sigma}_{\rm LO}^{(8)}\frac{\alpha_s}{\pi}\frac{(1-r)^{-2\epsilon}r^{\epsilon}}{\Gamma(1-\epsilon)}\left(\frac{4\pi\mu_r^2}{s}\right)^{\epsilon}&\left\{-\frac{C_A}{2\epsilon^2}-\frac{2C_A+\beta_0}{4\epsilon}+\frac{\beta_0}{4}\ln\frac{\mu_r^2}{m_c^2}+\frac{C_A(2-r)-2C_F(2+r)}{8(1-r)}\ln^2\frac{1-\sqrt{1-r}}{1+\sqrt{1-r}}\right.\\&+\frac{3(C_A-2C_F)}{2\sqrt{1-r}}\ln\frac{1-\sqrt{1-r}}{1+\sqrt{1-r}}+\frac{C_A(1-r)+2C_F}{4(1-r)}\left(\ln^2\frac{r}{2-r}+2{\rm Li}_2\frac{r}{2-r}\right)\\&\left.+\frac{-2C_A(2-r)+4C_F(3-2r)+(2-r)^2\beta_0}{2(2-r)^2}\ln\frac{r}{2(1-r)}+\frac{C_A(9+4\pi^2)}{6}-\frac{C_F[\pi^2(2-r)+6(1-r)(9-5r)]}{6(2-r)(1-r)}\right\}\\&\times\delta(1+r-z),\end{aligned} \tag{26}$$

where $\beta_0=\frac{11}{3}C_A-\frac{2}{3}n_f$ is the one-loop coefficient of the QCD β-function, and μ_r refers to the renormalization scale. Note here that the $1/\epsilon^2$ and $1/\epsilon$ poles, which sit exactly at $z=1+r$, are entirely of infrared origin.

C. Summing real and virtual corrections

We proceed to infer the net NLO radiative correction to $e^+e^-\to\gamma^*\to c\bar{c}({}^1S_0^{(8)})+g$, by adding up the real correction contributions, Eq. (19) from the $c\bar{c}({}^1S_0^{(8)})+gg$ channel and Eq. (23) from the $c\bar{c}({}^1S_0^{(8)})+q\bar{q}$ channel, together with the virtual correction in Eq. (26):

$$\begin{aligned}\frac{d\hat{\sigma}_{\rm NLO}^{(8)}}{dz}&\equiv\frac{d\hat{\sigma}_{\rm LO}^{(8)}}{dz}+\frac{d\hat{\sigma}_{\rm R}^{(8)}}{dz}+\frac{d\hat{\sigma}_{\rm V}^{(8)}}{dz}\\&=\frac{d\hat{\sigma}_{\rm LO}^{(8)}}{dz}+\frac{d\hat{\sigma}_{\rm R}^{(8),gg}}{dz}+\frac{d\hat{\sigma}_{\rm R}^{(8),q\bar{q}}}{dz}+\frac{d\hat{\sigma}_{\rm V}^{(8)}}{dz}.\end{aligned} \tag{27}$$

As anticipated, all the double and single IR poles indeed cancel, and we end up with the differential NLO SDC for the color-octet channel:

$$\begin{aligned}\frac{dF_8^{\rm NLO}}{dz}=&\frac{dF_8^{\rm LO}}{dz}+F_8^{\rm LO}\frac{\alpha_s}{\pi}\left\{\frac{\beta_0}{4}\ln\frac{\mu_r^2}{m_c^2}+\frac{C_A(2-r)-2C_F(2+r)}{8(1-r)}\ln^2\frac{1-\sqrt{1-r}}{1+\sqrt{1-r}}\right.\\&+\frac{3(C_A-2C_F)}{2\sqrt{1-r}}\ln\frac{1-\sqrt{1-r}}{1+\sqrt{1-r}}+\frac{C_A(1-r)+2C_F}{4(1-r)}\left(\ln^2\frac{r}{2-r}+2{\rm Li}_2\frac{r}{2-r}\right)\\&+\frac{-2C_A(2-r)+4C_F(3-2r)+(2-r)^2\beta_0}{2(2-r)^2}\ln\frac{r}{2(1-r)}-\frac{C_F[\pi^2(2-r)+6(1-r)(9-5r)]}{6(2-r)(1-r)}\\&\left.-2C_A\ln^2\frac{\sqrt{r}}{1+\sqrt{r}}+\frac{-23C_A+2n_f}{6}\ln\frac{\sqrt{r}}{1+\sqrt{r}}+\frac{121C_A+15\pi^2C_A-10n_f}{36}\right\}\delta(1+r-z)\\&+F_8^{\rm LO}\frac{\alpha_s}{\pi}\left\{\left[\frac{1}{1+r-z}\right]_+C_A\left[2\ln\frac{2-z+\sqrt{z^2-4r}}{2}-\ln\frac{z-\sqrt{z^2-4r}}{z+\sqrt{z^2-4r}}-\frac{2\sqrt{z^2-4r}}{1-r}\right.\right.\\&\left.+\frac{\sqrt{z^2-4r}(6+2r-6z+z^2)}{12(1-r)^3}\right]-C_A\left[\frac{\ln(1+r-z)}{1+r-z}\right]_++\frac{n_f}{6}\left[\frac{1}{1+r-z}\right]_+\left.\frac{(z^2-4r)^{3/2}}{(1-r)(2-z)^2}\right\}\\&+F_8^{\rm LO}\frac{\alpha_s}{\pi}\frac{C_A}{12(1-r)^3(z-2r)^3(2-z)^2}\left\{\sqrt{z^2-4r}[16r(3-9r+9r^2+24r^3-28r^4+9r^5)\right.\\&-8(3-3r-9r^2+120r^3-94r^4+27r^5)z+4(6-15r+162r^2-75r^3+22r^4)z^2\\&-2(3+90r+23r^2+4r^3)z^3+2(12+25r+3r^2)z^4-(9+5r)z^5+z^6]\\&+12(1-r)^2\ln\frac{z-2r-\sqrt{z^2-4r}}{z-2r+\sqrt{z^2-4r}}[4r(1-2r-6r^2+2r^3-3r^4)+8r^2(6+r+3r^2)z\\&\left.-2(1+12r+15r^2+12r^3)z^2+2(3+9r+8r^2)z^3-2(2+3r)z^4+z^5]\right\},\end{aligned}\tag{28}$$

where $F_8^{\rm LO}$ is given in Eq. (11).

After integrating Eq. (28) over the entire range of z, we then get the integrated NLO color-octet SDC:

$$\begin{aligned}F_8^{\rm NLO}=&F_8^{\rm LO}+F_8^{\rm LO}\frac{\alpha_s}{\pi}\left\{\frac{\beta_0}{4}\ln\frac{\mu_r^2}{m_c^2}+\frac{C_A(6-5r)-4C_F(2+r)}{16(1-r)}\ln^2\frac{1-\sqrt{1-r}}{1+\sqrt{1-r}}\right.\\&+\frac{C_A(28-27r)-36C_F(1-r)-4n_f}{12(1-r)^{3/2}}\ln\frac{1-\sqrt{1-r}}{1+\sqrt{1-r}}+C_A{\rm Li}_2\left(-\frac{1-r}{r}\right)\\&+\frac{C_A(1-r)+2C_F}{4(1-r)}\left(\ln^2\frac{r}{2-r}+2{\rm Li}_2\frac{r}{2-r}\right)+\frac{C_A(1-6\ln r)}{6(1-r)}-\frac{n_f(20-8r-9\ln r)}{18(1-r)}\\&+\frac{-2C_A(2-r)+4C_F(3-2r)+(2-r)^2\beta_0}{2(2-r)^2}\ln\frac{r}{2(1-r)}\\&\left.-\frac{C_F[\pi^2(2-r)+6(1-r)(9-5r)]}{6(2-r)(1-r)}+\frac{C_A(289+9\pi^2)}{36}\right\}.\end{aligned}\tag{29}$$

We note that the NLO radiative correction to $e^+e^-\to\gamma^*\to c\bar{c}({}^1S_0^{(8)})+g$ was already computed by Zhang *et al.* [51] about a decade ago. Those authors employed a purely numerical recipe and only presented the integrated partonic cross section. In contrast, we have presented the analytical expressions for both differential and integrated NLO color-octet SDCs [see Eqs. (28) and (29)]. When taking the same input parameters, our numerical prediction from Eq. (29) is consistent with theirs.

In the $\sqrt{s}\gg m_c$ limit, the correction for the color-octet SDC $\delta F_8\equiv F_8^{\rm NLO}-F_8^{\rm LO}$ reaches the following asymptotic form:

$$\delta F_8|_{\rm Asym} = F_8^{\rm LO}\frac{\alpha_s}{\pi}\left[\frac{\beta_0}{4}\ln\frac{\mu_r^2}{m_c^2}+\frac{C_A}{8}\ln^2 r-(2C_A-C_F)\ln 2\ln r+\frac{16C_A-9C_F-n_f}{6}\ln r\right.$$
$$\left.+\frac{7C_A-6C_F}{4}\ln^2 2-\frac{12C_A-9C_F-2n_f}{2}\ln 2+\frac{295C_A-162C_F-40n_f+3(C_A-2C_F)\pi^2}{36}\right]. \quad (30)$$

In contrast to the asymptotic form of $F_1^{\rm LO}(\mu_\Lambda)$ in Eq. (13), which is dominated by $\alpha_s^2 m_c \ln r/s^2$, here it is the double logarithm $\ln^2 r$ that accompanies the $\alpha_s^2 m_c/s^2$ factor. Since $\ln^2 r \gg |\ln r|$ in asymptotically high energy, one may conclude that the color-octet channel dominates the inclusive h_c production rate over the color-singlet one, at sufficiently high energy. The occurrence of $\ln^2 r$ at NLO strongly suggests that, in order to improve the reliability of the fixed-order predictions, it seems desirable to resum these types of double logarithms to all orders in α_s in the color-octet channel. We believe that the appropriate formalism to achieve this goal is to combine the double-parton fragmentation approach [52–54] and NRQCD factorization, where the large logarithms can be resummed by invoking the corresponding evolution equation. Practically speaking, at B factory energy, $\sqrt{s}\approx 10.6$ GeV, $\ln r$ is not particularly large, so resummation does not sound absolutely necessary. Nevertheless, in the next-generation e^+e^- colliders, as exemplified by CEPC and ILC, with $\sqrt{s}\approx 250$ GeV, the logarithms become so huge that one is forced to carry out this kind of resummation.

IV. END-POINT RESUMMATION FOR COLOR-OCTET CHANNEL

When we reach the end-point region in which $z\to 1+r$ and the h_c carries its maximally allowed energy, fixed-order calculations are plagued with large end-point logarithms of the form $\sum_{j<i}\alpha_s^i[\ln^{2i-j}(1+r-z)/(1+r-z)]_+$. This is clearly visible from those "+" distributions in our NLO color-octet prediction to the h_c energy spectrum in Eq. (28). To provide reliable predictions, these threshold logarithms have to be resummed to all orders. In this section we resum those logarithms to the NLL accuracy within the SCET framework [34–39].

Following Ref. [33], the factorization theorem for the color-octet h_c production is found to take the form

$$\frac{d\sigma}{dz'} = \hat{\sigma}_{\rm LO}^{(8)} H[\mu_H,\mu]\int_{z'}^1 dx S[x,\mu_S,\mu_r] \times J[s(1+r)(x-z'),\mu_J,\mu_r], \quad (31)$$

where we have introduced

$$z' = \frac{E_{h_c}}{E_{h_c}^{\rm max}} = \frac{z}{1+r}. \quad (32)$$

Here H is the hard function normalized to 1. The hard function which encodes the virtual corrections can be calculated perturbatively. Its one-loop results and anomalous dimension γ_H can be extracted from Eq. (26). S and J stand for the shape and jet functions, respectively.

The shape function $S^{(8,^1S_0)}(\ell^+)$ is defined in terms of ultrasoft fields that carry $\mathcal{O}(\Lambda_{\rm QCD})$ momentum:

$$S(\ell^+) = \frac{\langle 0|\chi^\dagger T^a\psi a_{h_c}^\dagger a_{h_c}\delta(\ell^+ - in\cdot D)\psi^\dagger T^a\chi|0\rangle}{4m_c\langle\mathcal{O}_8^{h_c}(^1S_0)\rangle}. \quad (33)$$

Its normalization is written as $\int d\ell^+ S(\ell^+)=1$. The ultrasoft covariant derivative can be expressed as $D^\mu = \partial^\mu - ig_s A_{us}^\mu$ and the lightlike vectors are defined as $n^\mu = (1,0,0,-1)$ and $\bar{n}^\mu = (1,0,0,1)$. χ and ψ are the Pauli spinors as previously introduced in Eq. (2), and $a_{h_c}^\dagger a_{h_c}$ is the projector to project onto the final h_c state.

The jet function describes the collinear radiation's recoil against the h_c in the threshold region. The jet function is independent of the state of the charm quark–antiquark pair and is defined as

$$J(\bar{n}\cdot p n\cdot k + p_\perp^2) = -\frac{s(1+r)}{4\pi}{\rm Im}\left[i\int d^4y e^{ik\cdot y}\langle 0|T\{{\rm Tr}[T^a B_\perp^{(0)\beta}(y)] \times {\rm Tr}[T^a B_{\perp\beta}^{(0)}(0)]\}|0\rangle\right], \quad (34)$$

where the subscript $\perp$ denotes the perpendicular direction; the superscript (0) denotes the bare field; and $B_\perp^\mu$ is the collinear gauge invariant effective field, which can be written as

$$B_\perp^\mu = \frac{1}{g_s}W^\dagger(\mathcal{P}_\perp^\mu + g_s(A_{n,q}^\mu)_\perp)W, \quad (35)$$

with a collinear gluon field $A_{n,q}^\mu$ and a collinear Wilson line $W_n(x)=\sum_{\rm perms}\exp(-g_s\frac{1}{\bar{\mathcal{P}}}\bar{n}\cdot A_{n,q}(x))$. Here $\mathcal{P}$ is the projection operator which picks out the large component of the momenta to its right [35].

The one-loop anomalous dimension γ_J for the jet function can be found in Ref. [33], while the anomalous dimension for the soft function can be inferred from the consistency condition $\gamma_S+\gamma_H+\gamma_J=0$.

To resum the large end-point logarithms, all components H, J, and S in the factorization theorem will be evolved

from their natural scales μ_H, μ_J, and μ_S to a common scale μ_r to evaluate the cross section, following the RGE

$$\frac{dF_i}{d\ln\mu} = \gamma_i F_i, \tag{36}$$

where i runs over the hard (H), collinear (J), and soft (S) modes. The scales μ_H, μ_J, and μ_S set the initial condition for the RG running and are chosen to minimize the logarithms in the higher order corrections to H, J, and S, respectively, which are found to be of order

$$\mu_H \sim \frac{s}{M}(1-r), \qquad \mu_S \sim M\frac{1+r}{1-r}(1-z'), \qquad \mu_J \sim \sqrt{\mu_H \mu_S}, \tag{37}$$

where we have introduced the mass of the heavy quark pair $M \equiv 2m_c$. After combining all pieces and assuming $\mu_J = \sqrt{\mu_H\mu_S}$, we arrived at a compact form for the NLL cross section, which reads

$$\frac{d\sigma^{\rm NLL}_{\rm pert}}{dz'} = \sigma^{(8)}_{\rm LO} e^h \left[\frac{\mu_H M}{s(1-r)}\right]^{2C_A A_\gamma[\mu_H,\mu_J]} \left[\frac{\mu_S}{M}\frac{1-r}{1+r}\right]^{\omega} \times \frac{e^{\omega\gamma_E}}{\Gamma[1-\omega]}(1-z')^{-\omega}, \tag{38}$$

where γ_E is the Euler constant. We define the auxiliary parameters

$$\begin{aligned} h &= 2C_A\bar{S}(\mu_H,\mu_r) - A_H(\mu_H,\mu_r) + 2C_A\bar{S}(\mu_S,\mu_r) \\ &\quad - A_S(\mu_S,\mu_r) - 4C_A\bar{S}(\mu_J,\mu_r) - A_J(\mu_J,\mu_r), \\ \omega &= 2C_A A_\gamma[\mu_S,\mu_J] < 0. \end{aligned} \tag{39}$$

In Eq. (39), $\bar{S}$ and A_i are found to be

$$\bar{S}(\mu_i,\mu_f) = \left[\frac{4\pi}{\alpha_s(\mu_i)}\left(1-\frac{1}{\rho}-\ln\rho\right) + \frac{\beta_1}{2\beta_0}\ln^2\rho + (1-\rho+\ln\rho)\left(\frac{\gamma_1}{\gamma_0}-\frac{\beta_1}{\beta_0}\right)\right]\frac{\gamma_0}{4\beta_0^2}, \tag{40a}$$

$$A_\gamma(\mu_i,\mu_f) = \frac{\gamma_0}{2\beta_0}\left[\ln\rho + \frac{\alpha_s(\mu_i)}{4\pi}\left(\frac{\gamma_1}{\gamma_0}-\frac{\beta_1}{\beta_0}\right)(\rho-1)\right], \tag{40b}$$

where

$$\rho = \frac{\alpha_s(\mu_f)}{\alpha_s(\mu_i)}, \tag{41a}$$

$$\beta_0 = \frac{11}{3}C_A - \frac{2}{3}n_f, \tag{41b}$$

$$\beta_1 = \frac{34}{3}C_A^2 - \frac{20}{3}C_A T_F n_f - 4C_F T_F n_f, \tag{41c}$$

$$\gamma_0 = 4, \tag{41d}$$

$$\gamma_1 = \left(\frac{67}{9}-\frac{\pi^2}{3}\right)C_A - \frac{20}{9}T_F n_f. \tag{41e}$$

Up to NLL accuracy, A_H, A_J, and A_S are obtained by truncating out the α_s term and replacing γ_0 in A_γ with γ_0^H, γ_0^J, or γ_0^S:

$$\gamma_0^H = -\frac{34}{3}C_A + \frac{4}{3}n_f, \quad \gamma_0^J = 2\beta_0, \quad \gamma_0^S = -\gamma_H^0 - \gamma_0^J = 4C_A. \tag{42}$$

Last we note that when $(1-z') \sim \mathcal{O}(\Lambda_{\rm QCD}/M)$, the process-independent shape function becomes nonperturbative and therefore a nonperturbative model $\mathcal{S}_{\rm non-pert}$.. is required for describing the nonperturbative soft radiation, and the resummed cross section is modified as

$$\frac{d\sigma^{\rm NLL}}{dz'} = \int_{z'}^1 \frac{dx}{x}\frac{d\sigma^{\rm NLL}_{\rm pert}}{dx}\mathcal{S}_{\rm non-pert}\left(\frac{z'}{x}\right), \tag{43}$$

where the nonperturbative shape function is adopted by a modified version of a model used in the decay of B mesons [55],

$$\mathcal{S}_{\rm non-pert}(\ell^+) = \frac{1}{\bar{\Lambda}}\frac{A^{AB}}{\Gamma(AB)}(x-1)^{AB-1}e^{-A(x-1)}, \tag{44}$$

with $x = \ell^+/\bar{\Lambda}$ and $\bar{\Lambda} \sim \mathcal{O}(\Lambda_{\rm QCD})$. Due to a lack of data, the parameters A and B have large uncertainties. However, the moments of the shape function can be expressed by the NRQCD operators and can be ordered by the power counting rules. The Nth moment of the shape function is $\mathcal{O}(\Lambda^N_{\rm QCD})$. According to the above model for the nonperturbative shape function, we have

$$\int_{\bar{\Lambda}}^\infty d\ell^+ \mathcal{S}_{\rm non-pert}(\ell^+) = 1, \tag{45}$$

$$\int_{\bar{\Lambda}}^\infty d\ell^+ \mathcal{S}_{\rm non-pert}(\ell^+)\ell^+ = \bar{\Lambda}(B+1), \tag{46}$$

$$\int_{\bar{\Lambda}}^\infty d\ell^+ \mathcal{S}_{\rm non-pert}(\ell^+)(\ell^+)^2 = (\bar{\Lambda})^2\left(\frac{B}{A}+(B+1)^2\right). \tag{47}$$

Thus the parameters A and B can be ordered as $A \sim B \sim \mathcal{O}(1)$. Future measurements shall be helpful to fit these two parameters.

V. NUMERICAL RESULTS

In this section, we present the numerical predictions for the differential and integrated cross sections for the

TABLE I. Numerical results for the integrated cross sections (fb) at $\sqrt{s} = 10.58$ GeV, from various perturbative levels. To assess the impact of the color-octet LDME on the cross sections, we list different results by varying the value of $\langle \mathcal{O}_8^{h_c(1P)}(^1S_0)\rangle$.

Refs.	$\langle \mathcal{O}_8^{h_c(1P)}(^1S_0)\rangle$ (GeV^3)	$\sigma_{\rm LO}^{(1)}$	$\sigma_{\rm LO}^{(8)}$	$\sigma_{\rm NLO}^{(8)}$	$\sigma_{\rm total}$
[61,62]	0.7×10^{-2}	−9.73	69.41	127.09	117.36
[60]	0.98×10^{-2}		97.17	177.92	168.20
[59]	1.6×10^{-2}		158.64	290.49	280.76

inclusive h_c production at the Belle II experiment, $\sqrt{s} = 10.58$ GeV. We adopt the running QED coupling constant $\alpha(\sqrt{s}) = 1/130.9$ [56]. We take the charm quark mass $m_c = 1.5$ GeV and the characteristic hadronic scale $\Lambda_{\rm QCD} = 332$ MeV [7]. For the process under consideration, we take the QCD renormalization scale $\mu_r = \sqrt{s}/2 = 5.29$ GeV, and we take the default value of the strong coupling constant $\alpha_s(\mu_r) = \alpha_s(\sqrt{s}/2) = 0.19$, which is determined by the two-loop RGE formula [57,58].

By definition in Eq. (1), the total cross section $\sigma_{\rm total}$ is obtained by summing the contributions from both color-singlet and octet channels, where the NLO QCD correction is included for the latter. For the LDMEs in Eq. (1), we take $\langle \mathcal{O}_1^{h_c(1P)}(^1P_1)\rangle = 0.32$ GeV^5 [10,59] in the color-singlet $h_c(1P)$ production. In contrast, the color-octet LDME $\langle \mathcal{O}_8^{h_c(1P)}(^1S_0)\rangle$ is poorly known, which bears a large uncertainty. In Table I, we present some benchmark choices for the color-octet LDME $\langle \mathcal{O}_8^{h_c(1P)}(^1S_0)\rangle$ and the corresponding integrated cross sections from different channels. In Fig. 2, we also show the dependence of the integrated (total) cross section on the renormalization scale μ_r and the color-octet LDME. In other places of the paper, we will fix the value of this color-octet LDME as $\langle \mathcal{O}_8^{h_c(1P)}(^1S_0)\rangle = 0.98 \times 10^{-2}$ GeV^3 [60], defined at the NRQCD factorization scale $\mu_\Lambda = m_c$.

From Table I and Fig. 2, we find that the $h_c(1P)$ production cross section at $\sqrt{s} = 10.58$ GeV is rather sensitive to the color-octet LDME. Therefore, the future measurements of the inclusive $h_c(1P)$ production at Belle II may provide a good place to unearth the value of this color-octet LDME.

In Fig. 3, we also show the scale dependence of the integrated cross sections from each production channel, at various perturbative levels. The scale μ_r is varied from $2m_c$ to $\sqrt{s}$. From Table I and Fig. 3, one sees that the NLO QCD correction to the color-octet channel is important, with a K-factor of about 1.8, and the color-octet contribution dominates the total production rate. It is noteworthy that the color-singlet contribution in the $\overline{\rm MS}$ scheme even becomes negative.

To date, the Belle I experiment has accumulated an integrated luminosity about 711 fb^{-1} at $\sqrt{s} = 10.58$ GeV. Thus, from our calculation, around $(0.8 - 2) \times 10^5$ $h_c(1P)$ events should have already been produced. Furthermore, we expect that roughly $(6 - 14) \times 10^6$ $h_c(1P)$ events will be produced, when the designed luminosity reaches 50 ab^{-1} at $\sqrt{s} = 10.58$ GeV in the forthcoming Belle II experiment.

Such a huge data set of $h_c(1P)$ events may allow experimentalists to accurately measure the $h_c(1P)$ differential energy spectrum. The $h_c(1P)$ energy distribution from the fixed-order prediction is plotted in Fig. 4, where the endpoint enhancement near $z \to 1 + r$ can be readily visualized, indicating the breakdown of the fixed-order perturbative prediction near the maximal energy of $h_c(1P)$.

For the color-octet channel, the large end-point logarithms have been resummed to the NLL accuracy within the SCET framework, as expounded in Sec. IV, and the

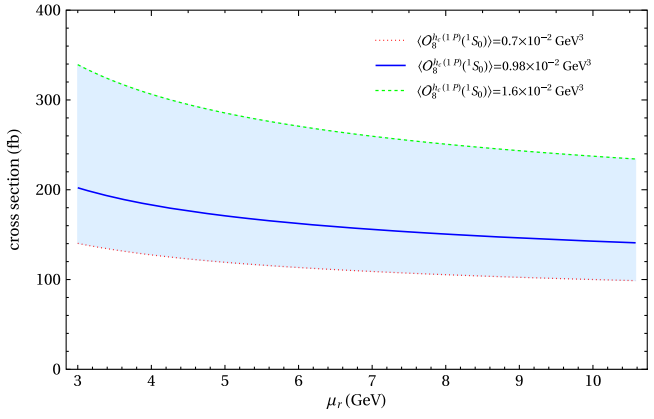

FIG. 2. The dependence of total cross section $\sigma_{\rm total}$ on the renormalization scale μ_r and color-octet LDME $\langle \mathcal{O}_8^{h_c(1P)}(^1S_0)\rangle$. The scale μ_r is varied from $2m_c$ to $\sqrt{s}$ and the band represents the theoretical uncertainty due to the variation of the color-octet LDME.

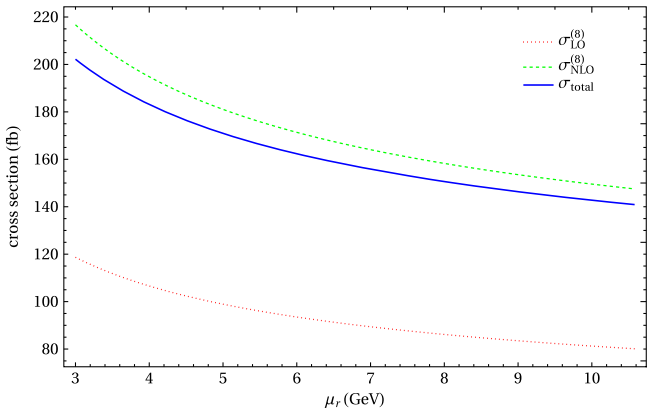

FIG. 3. The dependence of the inclusive $h_c(1P)$ production cross sections on the renormalization scale μ_r, at various levels of perturbative orders. μ_r ranges from $2m_c$ to $\sqrt{s}$. We have fixed the color-octet LDME $\langle \mathcal{O}_8^{h_c(1P)}(^1S_0)\rangle = 0.98 \times 10^{-2}$ GeV^3.

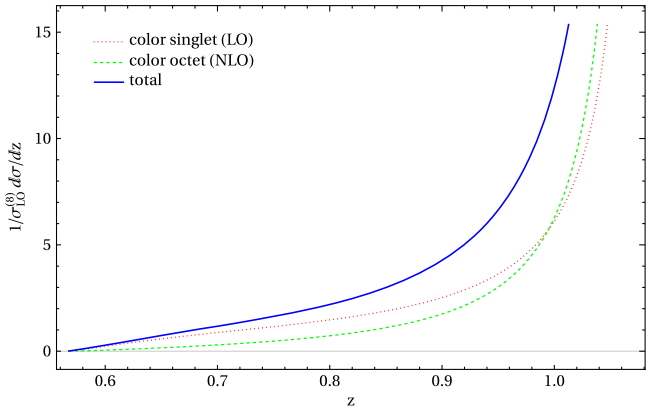

FIG. 4. The $h_c(1P)$ energy spectrum at $\sqrt{s} = 10.58$ GeV from the fixed-order calculation. In addition to their sum, we have also shown the contributions from the color-singlet channel at LO and the color-octet channel at NLO, all of which are normalized by the LO color-octet cross section $\sigma_{\rm LO}^{(8)}$.

end-point divergence problem can be resolved accordingly. Away from the end-point region, we merge the scales $\mu_S = \mu_H = \mu_J = \mu_r$ to turn off the resummation effect. While near the end point, we truncate the soft scale μ_S to around 1 GeV, to avoid the Landau pole. To account for the nonperturbative effects, we implement the shape function model following Refs. [33,55]. To merge all the scales to μ at small values of z, we adopted a "profile function" which smoothly turns on resummation when z is small and turns off resummation by setting all the scales equal to μ. The profile function are chosen as $\frac{1\pm\tanh(15(z'-z'_{\rm th}))}{2}$ [63]. The explicit form of $\mu_H(z)$ and $\mu_S(z)$ become $\mu_H(z) = \frac{1-\tanh(15(z'-z'_{\rm th}))}{2}\mu_r + \frac{1+\tanh(15(z'-z'_{\rm th}))}{2}\frac{s}{2m_c}(1-r)$ and $\mu_s(z) = \frac{1-\tanh(15(z'-z'_{\rm th}))}{2}\mu_r + \frac{1+\tanh(15(z'-z'_{\rm th}))}{2}$, where $z' = (1+r)z$ and $z'_{\rm th}$ is set to 0.85. We further match the NLL resummation with the NLO results to obtain the prediction for the full spectrum. The NLO + NLL differential cross section is plotted in Fig. 5, where four sets of parameters for the shape function are adopted, $(A = 5/2, B = 3/2)$; $(A = 3, B = 2)$; $(A = 5, B = 3)$; and $(A = 6, B = 4)$, respectively. We can see that the unphysical enhancement near the kinematic end point is removed after taking the resummation and shape function into account.

It is curious whether and how the $h_c(2P)$ meson, the first radially excited spin-singlet P-wave charmonium, could be observed at the super B factory. To reconstruct the potential $h_c(2P)$ events, one potentially useful decay chain is $h_c(2P) \to \eta_c(2S)\gamma$, followed by $\eta_c(2S) \to h_c(1P)\gamma$, $h_c(1P) \to \eta_c\gamma$, and $\eta_c \to K^+K^-\pi^0$. The decay chain, $h_c(2P) \to \eta_c(2S)\gamma$, followed by $\eta(2S) \to K\bar{K}\pi$, may be

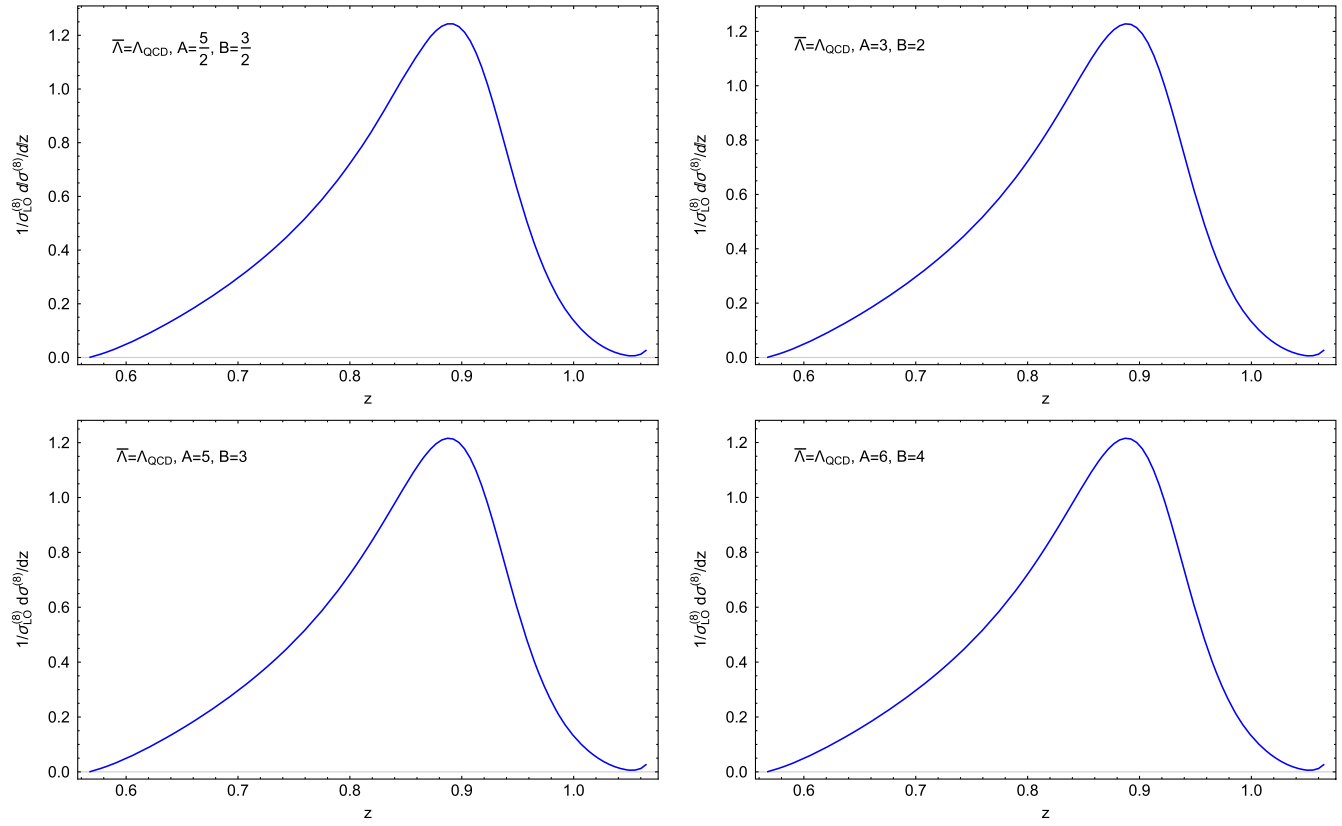

FIG. 5. The NLO + NLL predictions for the $h_c(1P)$ energy spectrum solely from the color-octet channel. We have taken different numerical inputs for the parameters A and B first introduced in Eq. (44).

another good channel for hunting the $h_c(2P)$. These decay channels are relatively clean, which hopefully will be helpful for hunting the elusive $h_c(2P)$ state.

The theoretical formulas for $h_c(1P)$ can be readily transplanted to predict the inclusive production rate of the $h_c(2P)$ meson. We adopt the color-singlet LDME $\langle \mathcal{O}_1^{h_c(2P)}(^1P_1)\rangle = 0.438\ \mathrm{GeV}^5$ [20,64]. It is rather difficult to accurately pin down the value of the color-octet LDME for $h_c(2P)$. We follow the very rough estimation based on the RGE in Refs. [10,20] and take $\langle \mathcal{O}_8^{h_c(2P)}(^1S_0)\rangle \approx 0.013\ \mathrm{GeV}^3$. With these input parameters, and ignoring the small difference in phase space integration, we then estimate the total cross section of $h_c(2P)$ to be around 224 fb at $\sqrt{s} = 10.58$ GeV. When the integrated luminosity reaches 711 fb^{-1} (50 ab^{-1}) at this specific energy, around 1.6×10^5 (1.1×10^7) $h_c(2P)$ events are expected to be produced. The energy spectrum of the $h_c(2P)$ state assumes a similar shape as plotted in Fig. 5.

VI. SUMMARY

In this paper, we evaluate the NLO perturbative correction to the color-octet h_c inclusive production in e^+e^- annihilation at the super B factory, within the NRQCD factorization framework. We are able to deduce the analytic NLO color-octet SDC in a closed form. The NLO correction from the color-octet channel is found to be positive and important. Around 10^7 $h_c(1P)$ and $h_c(2P)$ events are expected with the projected 50 ab^{-1} luminosity at $\sqrt{s} = 10.58$ GeV in the forthcoming Belle II experiment. It will be interesting to observe these P-wave spin-singlet states in the inclusive production process.

Nevertheless, the h_c energy spectrum predicted from the NLO calculation is plagued with the end-point singularity, which implies the failure of the fixed-order calculation near the maximal energy of h_c. With the aid of the SCET formalism, these large end-point logarithms are resummed to the NLL accuracy. Consequently, in conjunction with the nonperturbative shape function, we obtain the well-behaved predictions for the h_c energy spectrum in the entire kinematic range, which are awaiting close examination by the forthcoming Belle II experiment.

ACKNOWLEDGMENTS

We are grateful to Cheng-Ping Shen for several useful discussions on experimental aspects. X. L. would like to thank the Kavli Institute of Theoretical Physics in Santa Barbara for the hospitality during the completion of this manuscript. This work was supported in part by the National Natural Science Foundation of China under Grants No. 11375168, No. 11475188, No. 11621131001 (CRC110 by DGF and NSFC), and No. 11705092; by the Open Project Program of State Key Laboratory of Theoretical Physics under Grant No. Y4KF081CJ1; by the IHEP Innovation Grant under Contract No. Y4545170Y2; and by the State Key Lab for Electronics and Particle Detectors.

APPENDIX: ANALYTIC INTEGRATION OVER THE THREE-BODY PHASE SPACE

In this Appendix, we explain how we derive the differential color-octet cross sections in Eq. (19) in DR. Recall that the three-body phase space for $e^+e^- \to c\bar{c}(^1S_0^{(8)}) + gg(q\bar{q})$ in $d = 4 - 2\epsilon$ dimensions can be expressed as [20]

$$\begin{aligned}\int d\Phi_3 &= \frac{c_\epsilon (4\pi)^\epsilon}{\Gamma(1-\epsilon)}\left(\frac{s}{2}\right)^{1-2\epsilon}\frac{1}{(4\pi)^3}\int_{2\sqrt{r}}^{1+r} dz \int_{a-b}^{a+b} dx_1 x_1^{-2\epsilon}(z^2-4r)^{-\epsilon}(1-\cos^2\theta)^{-\epsilon} \\ &= \frac{c_\epsilon (4\pi)^\epsilon}{\Gamma(1-\epsilon)}\left(\frac{s}{2}\right)^{1-2\epsilon}\frac{1}{(4\pi)^3}\int_{2\sqrt{r}}^{1+r} dz \int_{a-b}^{a+b} dx_1 2^{-2\epsilon}(1+r-z)^{-\epsilon}(x_1-a+b)^{-\epsilon}(a+b-x_1)^{-\epsilon} \\ &= \frac{c_\epsilon (4\pi)^\epsilon}{\Gamma(1-\epsilon)}\frac{s^{1-2\epsilon}}{2}\frac{1}{(4\pi)^3}\int_{2\sqrt{r}}^{1+r} dz(1+r-z)^{-\epsilon}\int_{-b}^{b} d\eta(b+\eta)^{-\epsilon}(b-\eta)^{-\epsilon}, \end{aligned} \tag{A1}$$

where c_ϵ is introduced in Eq. (6), and θ is the polar angle between $\mathbf{k}_1$ and $\mathbf{P}$:

$$\cos\theta = \frac{2(1+r-z) - x_1(2-z)}{x_1\sqrt{z^2-4r}}. \tag{A2}$$

In Eq. (A1), we have introduced three auxiliary variables a, b, and η,

$$a = \frac{2-z}{2}, \quad b = \frac{\sqrt{z^2-4r}}{2}, \quad \text{and} \quad \eta = x_1 - a, \tag{A3}$$

which satisfy $a^2 - b^2 = 1 + r - z$.

First, let us concentrate on the soft term $\mathcal{I}_S(x_i, z)$ in Eq. (16a). Upon integrating over the energy fraction of gluon 1, it will result in a single IR pole. For the sake of clarity, we discard the irrelevant perfectors in Eq. (A1) and consider the following integral:

$$\mathcal{A}_S \equiv \int_{a-b}^{a+b} dx_1 \frac{(1+r-z)^{-\epsilon}(x_1-a+b)^{-\epsilon}(a+b-x_1)^{-\epsilon}}{(1+r-z-x_1)^2},$$
$$= \frac{1}{(1+r-z)^{1+2\epsilon}} \int_{a-b}^{a+b} dt \frac{(1-\frac{a-b}{t})^{-\epsilon}(\frac{a+b}{t}-1)^{-\epsilon}}{(1-t)^2}. \tag{A4}$$

In the second line, we change the integration variable from x_1 to t [20],

$$t = \frac{1+r-z}{x_1}, \tag{A5}$$

which lies in the range

$$0 < a-b < t < a+b < 1-r. \tag{A6}$$

To explicitly identify the IR pole in $\mathcal{A}_S$, we can rewrite [20]

$$\frac{1}{(1+r-z)^{1+2\epsilon}} = -\frac{\delta(1+r-z)}{2\epsilon(1-\sqrt{r})^{4\epsilon}} + \left[\frac{1}{1+r-z}\right]_+ - 2\epsilon\left[\frac{\ln(1+r-z)}{1+r-z}\right]_+ + \mathcal{O}(\epsilon^2), \tag{A7}$$

where the "+"-function is defined in Eq. (20).

Now the integration over t in Eq. (A4) is convergent, therefore one can expand the integrand in powers of ϵ. Through the order-ϵ^0, $\mathcal{A}_S$ bears the following form:

$$\mathcal{A}_S = \left\{-\frac{1-r}{2r\epsilon} + \frac{(1-r)[4\ln(1-\sqrt{r})+\ln r]}{2r}\right\}\delta(1+r-z) + \left[\frac{1}{1+r-z}\right]_+ \frac{\sqrt{z^2-4r}}{r} + \mathcal{O}(\epsilon). \tag{A8}$$

The soft-collinear term $\mathcal{I}_{SC}(x_i, z)$ in Eq. (16c) would result in a double IR pole upon phase space integration. To facilitate the extraction of the IR poles, we first observe that $\mathcal{I}_{SC}$ contains the following term:

$$\frac{1}{(1+r-z)(1+r-z-x_1)} = \frac{1}{x_1(1+r-z-x_1)} - \frac{1}{x_1(1+r-z)}, \tag{A9}$$

which can be decomposed into two pieces through a partial fraction.

The first term in Eq. (A9) only leads to a soft singularity. Following the trick of changing the variable in Eq. (A4), we can readily work out the following integration in DR:

$$\mathcal{A}'_S = \int_{a-b}^{a+b} dx_1 \frac{(1+r-z)^{-\epsilon}(x_1-a+b)^{-\epsilon}(a+b-x_1)^{-\epsilon}}{x_1(1+r-z-x_1)}$$
$$= \frac{1}{(1+r-z)^{1+2\epsilon}} \int_{a-b}^{a+b} dt \frac{(1-\frac{a-b}{t})^{-\epsilon}(\frac{a+b}{t}-1)^{-\epsilon}}{t-1}$$
$$= \left\{-\frac{\ln r}{2\epsilon} + \frac{\ln r}{4}[\ln r + 8\ln(1-\sqrt{r})]\right\}\delta(1+r-z) + \left[\frac{1}{1+r-z}\right]_+ \ln\frac{z-\sqrt{z^2-4r}}{z+\sqrt{z^2-4r}} + \mathcal{O}(\epsilon). \tag{A10}$$

The second term in Eq. (A9) would lead to a double IR pole upon integration over x_1. We then face the following integral:

$$\mathcal{A}_{SC} = \int_{a-b}^{a+b} dx_1 \frac{(1+r-z)^{-\epsilon}(x_1-a+b)^{-\epsilon}(a+b-x_1)^{-\epsilon}}{x_1(1+r-z)}$$
$$= \frac{1}{(1+r-z)^{1+\epsilon}} \int_{a-b}^{a+b} dx_1 \frac{(x_1-a+b)^{-\epsilon}(a+b-x_1)^{-\epsilon}}{x_1}$$
$$= \frac{1}{(1+r-z)^{1+\epsilon}} \int_{-b}^{b} d\eta \frac{(\eta+b)^{-\epsilon}(b-\eta)^{-\epsilon}}{\eta+a}. \tag{A11}$$

In the last step, we have switched the integration variable from x_1 to η, as specified in the last line of Eq. (A1).

The integration over η can be done in a straightforward way:

$$\int_{-b}^{b} d\eta \frac{(\eta+b)^{-\epsilon}(b-\eta)^{-\epsilon}}{\eta+a} = \frac{\sqrt{\pi}b^{1-2\epsilon}\Gamma(1-\epsilon)\,{}_2F_1(\frac{1}{2},1;\frac{3}{2}-\epsilon;\frac{b^2}{a^2})}{a\Gamma(\frac{3}{2}-\epsilon)}$$
$$= \frac{\sqrt{\pi}b^{1-2\epsilon}\Gamma(-\epsilon)\,{}_2F_1(\frac{1}{2},1;1+\epsilon;1-\frac{b^2}{a^2})}{a\Gamma(\frac{1}{2}-\epsilon)} + \pi\csc(\pi\epsilon)(a^2-b^2)^{-\epsilon}, \tag{A12}$$

where ${}_2F_1$ represents the Gauss hypergeometric function. The singularity associated with the $\epsilon \to 0$ limit can be readily traced in this format, which stems from $\Gamma(-\epsilon)$ and $\csc(\pi\epsilon)$. With the aid of the package HypExp [65], we find the following expansion formula particularly useful:

$$ {}_2F_1\left(\frac{1}{2},1;1+\epsilon;1-\frac{b^2}{a^2}\right)=\frac{a}{b}\left(1+2\epsilon\ln\frac{2b}{a+b}\right)+\mathcal{O}(\epsilon^2). \tag{A13}$$

Combining the distribution identity in Eq. (A7), we can get

$$\begin{aligned}&\frac{1}{(1+r-z)^{1+\epsilon}}\frac{\sqrt{\pi}b^{1-2\epsilon}\Gamma(-\epsilon){}_2F_1(\frac{1}{2},1;1+\epsilon;1-\frac{b^2}{a^2})}{a\Gamma(\frac{1}{2}-\epsilon)}\\&=\left\{\frac{1}{\epsilon^2}-\frac{2\ln[(1-\sqrt{r})(1-r)]}{\epsilon}+2\ln^2[(1-\sqrt{r})(1-r)]-\frac{\pi^2}{6}\right\}\delta(1+r-z)\\&\quad+\left(-\frac{1}{\epsilon}+2\ln\frac{2-z+\sqrt{z^2-4r}}{2}\right)\left[\frac{1}{1+r-z}\right]_+ +\left[\frac{\ln(1+r-z)}{1+r-z}\right]_+ +\mathcal{O}(\epsilon),\end{aligned} \tag{A14a}$$

$$\begin{aligned}&\frac{1}{(1+r-z)^{1+\epsilon}}\pi\csc(\pi\epsilon)(a^2-b^2)^{-\epsilon}\\&=\left\{-\frac{1}{2\epsilon^2}+\frac{2\ln(1-\sqrt{r})}{\epsilon}-4\ln^2(1-\sqrt{r})-\frac{\pi^2}{12}\right\}\delta(1+r-z)+\frac{1}{\epsilon}\left[\frac{1}{1+r-z}\right]_+ -2\left[\frac{\ln(1+r-z)}{1+r-z}\right]_+ +\mathcal{O}(\epsilon).\end{aligned} \tag{A14b}$$

Adding these two pieces together, we arrive at the final expression for $\mathcal{A}_{\rm SC}$:

$$\begin{aligned}\mathcal{A}_{\rm SC}=&\left\{\frac{1}{2\epsilon^2}-\frac{2\ln(1-r)}{\epsilon}-4\ln^2(1-\sqrt{r})+2\ln^2[(1-\sqrt{r})(1-r)]-\frac{\pi^2}{4}\right\}\delta(1+r-z)\\&+2\ln\left(\frac{2-z+\sqrt{z^2-4r}}{2}\right)\left[\frac{1}{1+r-z}\right]_+ -\left[\frac{\ln(1+r-z)}{1+r-z}\right]_+ +\mathcal{O}(\epsilon).\end{aligned} \tag{A15}$$

The occurrence of a double IR pole is as anticipated, by examining the pole structure of Eq. (16c).

[1] T. A. Armstrong *et al.*, Phys. Rev. Lett. **69**, 2337 (1992).
[2] M. Andreotti *et al.*, Phys. Rev. D **72**, 032001 (2005).
[3] J. L. Rosner *et al.* (CLEO Collaboration), Phys. Rev. Lett. **95**, 102003 (2005).
[4] P. Rubin *et al.* (CLEO Collaboration), Phys. Rev. D **72**, 092004 (2005).
[5] M. Ablikim *et al.* (BESIII Collaboration), Phys. Rev. Lett. **104**, 132002 (2010).
[6] M. Ablikim *et al.* (BESIII Collaboration), Phys. Rev. D **86**, 092009 (2012).
[7] C. Patrignani *et al.* (Particle Data Group), Chin. Phys. C **40**, 100001 (2016).
[8] I. Adachi *et al.* (Belle Collaboration), Phys. Rev. Lett. **108**, 032001 (2012).
[9] W. E. Caswell and G. P. Lepage, Phys. Lett. **167B**, 437 (1986).
[10] G. T. Bodwin, E. Braaten, and G. P. Lepage, Phys. Rev. D **51**, 1125 (1995); **55**, 5853(E) (1997).
[11] N. Brambilla *et al.*, Eur. Phys. J. C **71**, 1534 (2011).
[12] V. A. Novikov, L. B. Okun, M. A. Shifman, A. I. Vainshtein, M. B. Voloshin, and V. I. Zakharov, Phys. Rep. **41**, 1 (1978).
[13] J. Z. Li, Y. Q. Ma, and K. T. Chao, Phys. Rev. D **88**, 034002 (2013).
[14] G. T. Bodwin, E. Braaten, T. C. Yuan, and G. P. Lepage, Phys. Rev. D **46**, R3703 (1992).
[15] M. Beneke, F. Maltoni, and I. Z. Rothstein, Phys. Rev. D **59**, 054003 (1999).
[16] S. Fleming and T. Mehen, Phys. Rev. D **58**, 037503 (1998); AIP Conf. Proc. **452**, 101 (1998).
[17] K. Sridhar, Phys. Lett. B **674**, 36 (2009).
[18] C. F. Qiao, D. L. Ren, and P. Sun, Phys. Lett. B **680**, 159 (2009).
[19] J. X. Wang and H. F. Zhang, J. Phys. G **42**, 025004 (2015).
[20] Y. Jia, W. L. Sang, and J. Xu, Phys. Rev. D **86**, 074023 (2012).
[21] J. X. Wang and H. F. Zhang, Phys. Rev. D **86**, 074012 (2012).

[22] G. Chen, X. G. Wu, Z. Sun, X. C. Zheng, and J. M. Shen, Phys. Rev. D **89**, 014006 (2014).
[23] L. B. Chen, J. Jiang, and C. F. Qiao, Chin. Phys. C **39**, 103101 (2015).
[24] R. Zhu, Phys. Rev. D **92**, 074017 (2015).
[25] F. Feng, S. Ishaq, Y. Jia, and J. Y. Zhang, arXiv:1712.09986.
[26] A. Abulencia *et al.* (CDF Collaboration), Phys. Rev. Lett. **99**, 132001 (2007).
[27] R. Aaij *et al.* (LHCb Collaboration), Eur. Phys. J. C **71**, 1645 (2011).
[28] G. Aad *et al.* (ATLAS Collaboration), Nucl. Phys. **B850**, 387 (2011).
[29] V. Khachatryan *et al.* (CMS Collaboration), Eur. Phys. J. C **71**, 1575 (2011).
[30] B. Abelev *et al.* (ALICE Collaboration), Phys. Rev. Lett. **108**, 082001 (2012).
[31] T. K. Pedlar *et al.* (CLEO Collaboration), Phys. Rev. Lett. **107**, 041803 (2011).
[32] M. Ablikim *et al.* (BESIII Collaboration), Phys. Rev. Lett. **118**, 092002 (2017).
[33] S. Fleming, A. K. Leibovich, and T. Mehen, Phys. Rev. D **68**, 094011 (2003).
[34] C. W. Bauer, S. Fleming, and M. E. Luke, Phys. Rev. D **63**, 014006 (2000).
[35] C. W. Bauer, S. Fleming, D. Pirjol, and I. W. Stewart, Phys. Rev. D **63**, 114020 (2001).
[36] C. W. Bauer and I. W. Stewart, Phys. Lett. B **516**, 134 (2001).
[37] C. W. Bauer, D. Pirjol, and I. W. Stewart, Phys. Rev. D **65**, 054022 (2002).
[38] C. W. Bauer, S. Fleming, D. Pirjol, I. Z. Rothstein, and I. W. Stewart, Phys. Rev. D **66**, 014017 (2002).
[39] M. Beneke, A. P. Chapovsky, M. Diehl, and T. Feldmann, Nucl. Phys. **B643**, 431 (2002).
[40] G. C. Nayak, J. W. Qiu, and G. F. Sterman, Phys. Lett. B **613**, 45 (2005).
[41] G. C. Nayak, J. W. Qiu, and G. F. Sterman, Phys. Rev. D **72**, 114012 (2005).
[42] A. Petrelli, M. Cacciari, M. Greco, F. Maltoni, and M. L. Mangano, Nucl. Phys. **B514**, 245 (1998).
[43] G. T. Bodwin, X. G. i Tormo, and J. Lee, Phys. Rev. D **81**, 114014 (2010).
[44] W. Y. Keung, Phys. Rev. D **23**, 2072 (1981).
[45] T. Hahn, Comput. Phys. Commun. **140**, 418 (2001).
[46] V. Shtabovenko, R. Mertig, and F. Orellana, Comput. Phys. Commun. **207**, 432 (2016).
[47] B. W. Harris and J. F. Owens, Phys. Rev. D **65**, 094032 (2002).
[48] F. Feng, Comput. Phys. Commun. **183**, 2158 (2012).
[49] A. V. Smirnov, Comput. Phys. Commun. **189**, 182 (2015).
[50] T. Hahn and M. Perez-Victoria, Comput. Phys. Commun. **118**, 153 (1999).
[51] Y. J. Zhang, Y. Q. Ma, K. Wang, and K. T. Chao, Phys. Rev. D **81**, 034015 (2010).
[52] S. Fleming, A. K. Leibovich, T. Mehen, and I. Z. Rothstein, Phys. Rev. D **86**, 094012 (2012).
[53] Z. B. Kang, Y. Q. Ma, J. W. Qiu, and G. Sterman, Phys. Rev. D **90**, 034006 (2014).
[54] Y. Q. Ma, J. W. Qiu, G. Sterman, and H. Zhang, Phys. Rev. Lett. **113**, 142002 (2014).
[55] A. K. Leibovich, Z. Ligeti, and M. B. Wise, Phys. Lett. B **539**, 242 (2002).
[56] G. T. Bodwin, J. Lee, and C. Yu, Phys. Rev. D **77**, 094018 (2008).
[57] T. van Ritbergen, J. A. M. Vermaseren, and S. A. Larin, Phys. Lett. B **400**, 379 (1997).
[58] K. G. Chetyrkin, J. H. Kuhn, and M. Steinhauser, Comput. Phys. Commun. **133**, 43 (2000).
[59] P. L. Cho and A. K. Leibovich, Phys. Rev. D **53**, 150 (1996).
[60] P. L. Cho and A. K. Leibovich, Phys. Rev. D **53**, 6203 (1996).
[61] Y. Q. Ma, K. Wang, and K. T. Chao, Phys. Rev. D **83**, 111503 (2011).
[62] B. Gong, L. P. Wan, J. X. Wang, and H. F. Zhang, Phys. Rev. Lett. **110**, 042002 (2013).
[63] X. Liu and F. Petriello, Phys. Rev. D **87**, 094027 (2013).
[64] E. J. Eichten and C. Quigg, Phys. Rev. D **52**, 1726 (1995).
[65] T. Huber and D. Maitre, Comput. Phys. Commun. **178**, 755 (2008).